Analyst

Accepted Manuscript

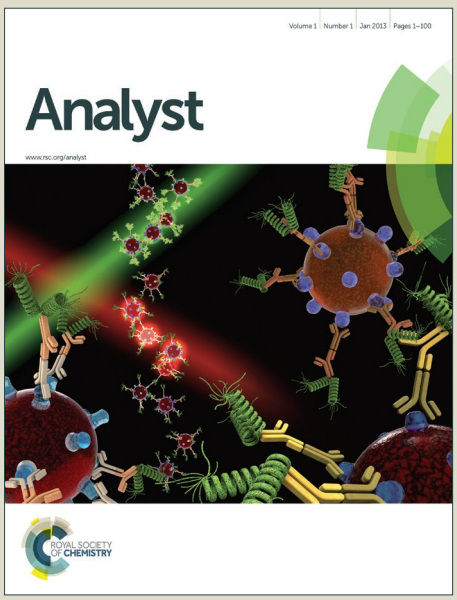

ROYAL SOCIETY OF CHEMISTRY

www.rsc.org/analyst

Analyst

RSCPublishing

ARTICLE

Raman microspectroscopy of the noncancerous and the cancerous human breast tissues. Identification and phase transitions of linoleic and oleic acids by Raman spectroscopy and Raman low-temperature studies†

Cite this: DOI: 10.1039/xoxxoooooox

Received ooth January 2012,
Accepted ooth January 2012

DOI: 10.1039/xoxxoooooox

www.rsc.org/

Beata Brozek-Pluska,[a,*] Monika Kopec,[a] Jakub Surmacki,[a] and Halina Abramczyk[a]

We present the results of Raman studies in the temperature range of 293-77 K on vibrational properties of the linoleic and oleic acids and Raman microspectroscopy of the human breast tissues at the room temperature. Our results confirmed the significant role of unsaturated fatty acids in differentiation of the noncancerous and the cancerous breast tissues and the role of vibrational spectroscopy in phase transitions identification. We have found that vibrational properties are very sensitive indicators to specify phases and phase transitions typical for unsaturated fatty acids at the molecular level. Using Raman spectroscopy we have identified high-temperature, middle-temperature and low-temperatures phases of linoleic acid. Results obtained for linoleic acid were compared with parameters characteristic for α and γ phases of oleic acid-the parent compound of polyunsaturated fatty acids.

Introduction

Polyunsaturated fats can have a positive effect on human health when consumed in moderation and when eaten to replace saturated and trans fats in a diet. In human body fatty acids are important sources of 'fuel' because their metabolism yield large quantities of ATP used by different types of cells in their life cycle.[1,2] In particular, heart and skeletal muscle prefer fatty acids than glucose as an energy source. Oleic acid is a monounsaturated ω-9 fatty acid found in various animal and vegetable fats, and what is relevant to this study, is a parent acid of many polyunsaturated fatty acids (PUFA) like: linoleic acid (LA), α-linolenic acid (ALA), eicosapentaenoic acid (EPA), and docosahexaenoic acid (DHA) from the ω-3 family, and γ-linolenic acid (GLA), dihomo-γ-linolenic acid (DGLA) and arachidonic acid (AA) from the ω-6 family.[2,3] The most important role of PUFA in human organisms is that they are precursors of eicosanoids called also tissue hormones.[2-9] These very unstable, rapidly decomposed substances can act as a triggering factor of cancer changes.[10-15] The type and amount of the synthesized eicosanoids are dependent on the availability of the precursor, activity of phospholipases A2 and C, cyclooxygenase and lipoxygenase. AA is a precursor of eicosanoids having a highest biological activity even in very small quantities. Eicosanoids produced via AA metabolism stimulate the development of atherosclerosis, thrombus formation, severe inflammation and allergic reactions, as well as cell proliferation and growth of cancer tissue, especially in the mammary gland, colon and prostate, but polyunsaturated fatty acids can play also the protective roles in cancer risk, the positive role of OA, LA, DHA and EPA in breast cancer risk have been proved in clinical trials.[16-26]

Even if the dietary factors contribution to the etiology of cancer has not been established unequivocally some research on social groups with varied eating habits show the correlation between the regional differences of breast cancer risk and diet. The fatty acid composition in breast tissue was directly associated with mammary cancer growth in many studies in animals and human cell lines.[27,28] cis-Polyunsaturated fatty acids such as LA and AA are also abundant in brain and retinal tissues for special properties originated form the cis-olefine group. Their unsaturation plays very important role in physical properties of biomembranes, nervous and optical human systems.[29-33]

The distribution and chemical characterization of fatty acids can be monitored in human tissues using Raman microspectroscopy. Raman mapping allows tracking of subcellular structures rich in lipids and fatty acids and represents the ideally suited technique to monitor inhomogeneous distribution of different tissues components. The advantage of Raman spectroscopy as compared to other

techniques is that none preparation of the tissues samples is needed and many compounds can be tracked simultaneously. Fatty acids are characterized by many intense Raman peaks and the level of unsaturation of these acids can be also easy monitored.[34-36]

In this paper we would like to focus on structure and conformational changes at molecular level of selected PUFA because such properties are still unknown and are crucial for their functions in biological systems.

Many lipids compounds with unsaturated acyl chains form several polymorphic phases that are sensitive for the number and the position of the double C=C bond.[37-44] Vibrational spectroscopy was used in the past for investigations concerning the phase transitions of palmitoleic, erucic and oleic acids. On the basis of a spectroscopic and other physical methods (DSC, density, viscosity, self-diffusion), it has been suggested that OA forms a quasi-smectic liquid crystal structure in the temperature range from the melting at 15 °C to about 30 °C, the structure between 30 °C and 55 °C consists of clusters with a less ordered structure, while the structure above 55 °C appears to be an isotropic liquid. Below the melting temperature the oleic acid exists in three solid state phases: α, β, γ. They have been identified by X-ray diffraction, vibrational spectroscopy, DSC. It has been found that the $\alpha - \gamma$ transition occurs at -2.2 °C and represents a disorder-order transition, where in the α phase, the alkyl chain on the methyl side of the C=C bond exhibits conformational disorder, while the segment on the carboxyl-side of C=C bond remains in the ordered all-trans conformation. The γ phase represents more ordered structure, in which the unit cell is pseudo-orthorhombic (space group *P21/a*) with four molecules (or two hydrogen bonded dimers) per unit cell. The molecules are bent at the C=C bond, and the hydrocarbon chains pack according to the orthorhombic $O_{\parallel}'$ subcell (space group *Pma2*). The β phase exists in two modifications: stable β1 and metastable β2. In the β1 phase the unit cell belongs to a triclinic system of *P1* where the asymmetric unit contains two crystallographically independent molecules A and B. The molecular layer exhibits a unique interdigitated structure, where the methyl group of the molecule A and the carboxyl group of the molecule B are located in the same plane. The methyl- and the carboxyl-sided chains together form a $T_{\parallel}$ subcell. The β phase is unique, has been found only in oleic acid and does not show an order-disorder type solid-state transition.[3,5,44-46]

Biological functions of linoleic acid has been investigated for elucidating its physiological and pathological roles also using different experimental methods including FTIR spectroscopy. However, the dynamical properties of LA have been still under investigations. DSC and XRD experiments confirm that LA forms three phases known as low temperature (LT), middle temperature (MT) and high temperature (HT) phases in the temperature region from -100 °C to -5 °C. On heating process the LT phase transforms to the MT phase at -51,3 °C and the MT phase transforms to the HT phase at -33.5 °C respectively. The thermodynamic parameters of both solid-state reversible phase transitions show that the transition enthalpy of the MT/HT phase transition is significantly smaller 0.26 kJ/mol than that of the LT/MT transition equal to 2.6 kJ/mol suggesting that the most important structural changes take place on the LT/MT transition. Both values are smaller than enthalpy of the α/γ phase transition of OA equal to 8.76 kJ/mol.[47-50]

The main goal of the present study is to investigate the structural changes in the LT/MT and MT/HT phase transitions of LA by low-temperature Raman spectroscopy and to discussed results with data obtained in our group for oleic acid.[35] In this paper we have used also Raman microspectroscopy at room temperature 293 K to investigate the cancerous and the noncancerous human breast tissues to correlate the lipid profile of these tissues with Raman spectra of OA and LA at 293 K.

We do believe that presented results should not only help in understanding the molecular mechanisms that drive cancer changes but also prove that vibrational spectroscopy can be used to follow phase transitions of biological important fatty acids.

Experimental methods

Unsaturated fatty acids

Unsaturated fatty acids: oleic acid (product number O1008) and linoleic acid (product number L1367), were purchased from Sigma-Aldrich and used without purification.

Patients and samples

We examined human breast cancer specimens (infiltrating ductal carcinoma). The breast tissue samples were obtained during a surgical operation. The research did not affect the course of the operation or treatment of the patients. Total number of patients was 232. Total number of samples was 464. For each patient the breast tissue from the safety margin and the tumor mass were measured and analyzed. The typical results of one of the patients have been used to illustrate the essential findings of research. To visualize and identify tissue structures we have used Raman imaging. We avoided the standard steps in the histology protocols, such as formalin fixation, paraffin-embedding, and coating to adhere the cover glass to the microscope slide, on Raman measurements. We observed that using the standard chemical fixative to preserve the tissue from degradation, i.e., 10% neutral-buffered formalin (4% formaldehyde in phosphate-buffered saline), did not introduce essential changes in the Raman spectra. This conclusion is based on a comparison between the results obtained using fresh tissue samples (>160 patients) and those obtained using formalin-fixed tissue samples (>60 patients). In contrast, paraffin embedding was not an appropriate protocol for use in Raman measurements. The paraffinization protocol contains steps, such as alcohol dehydration, xylene clearance, and paraffin wax infiltration and embedding that might introduce artifacts in Raman spectra. We observed that the use of frozen sections (cryosectioned samples), in which the frozen fresh tissue (or formalin-fixed tissue) is sliced into thin sections (16

μm) using a microtome, is the most appropriate protocol for Raman measurements. The fresh tissue obtained during surgery was snap frozen in liquid nitrogen. The frozen blocks of fresh tissue were stored at −80 °C until further processing. The thin slices without staining were placed on CaF_2 windows for Raman measurements. The adjacent sections of tissue were mounted on glass slides, stained with H&E and covered with another layer of glass using a specific adhesive (Histokitt, Glaswarenfabrik Karl Hecht GmbH & Co KG, CAS: 1330-20-7) for histological examination. After obtaining the Raman measurements, trained pathologists examined and stained the slices. As the quality of the slides produced from the frozen sections was lower than that obtained in the standard procedure, standard histology processing using wax-embedded tissue was additionally performed to obtain a more accurate diagnosis for each patient. Professional medical doctors, a board certified as pathologists, from the Medical University of Lodz, Department of Pathology, Chair of Oncology performed and analyzed the histological images. All procedures were conducted under a protocol approved by the Bioethical Committee at the Medical University of Lodz (RNN/45/14/KE/11/03/2014).[51]

Instrumentation

All Raman images and spectra reported in this study were acquired using a Ramanor U1000 Raman spectrometer (Jobin Yvon) excited with an ion Ar laser (514 nm) and with an alpha 300 RA (WITec, Ulm, Germany) model equipped with an Olympus microscope coupled via the fiber of a 50 μm core diameter to an UHTS (Ultra High Throughput Spectrometer) spectrometer and a CCD Camera Andor Newton DU970N-UVB-353 operating in standard mode with 1600 × 200 pixels at −60 °C with full vertical binning. The incident laser beam (doubled SHG of the Nd:YAG laser (532 nm)) of alpha 300 RA was focused on the sample through a 40× dry objective (Nikon, objective type CFI Plan Fluor C ELWD DIC-M, numerical aperture (NA) of 0.60 and a 3.6–2.8 mm working distance) to the spot of 600 nm. The average laser excitation power was 10 mW, with an integration time of 0.03 s. Rayleigh scattered light was removed using an edge filter. A piezoelectric table was used to record Raman images. Spectra were collected at one acquisition per pixel and 1200 lines per mm diffraction grating. Each spectrum was processed to remove cosmic rays, increase the signal-to-noise ratio via spectral smoothing (Savitzky–Golay method). Data acquisition and processing were performed using WITec Project 2.10.

Results and discussion

In this section, the results of the Raman studies on the noncancerous and the cancerous human breast tissues of the same patient P80 are presented.

The typical Raman spectra of the noncancerous and the cancerous (infiltrating ductal cancer, G3) breast tissues are presented in Figures 1 and 2.

Fig. 1 Microscopy, Raman images and Raman spectra of the noncancerous breast tissue of patient P80. A Microscopy image (500 × 500 μm) composed of several single video images of the noncancerous breast tissue, B Raman image (350 × 350 μm) of the cryosectioned noncancerous tissue from the region marked in A obtained by the basis analysis, C Raman spectra of the noncancerous breast tissue. The colours of the Raman spectra correspond to the colours in the Raman image. Mixed areas are displayed as mixed colours. Integration time: 0.03 s.[36]

Fig. 2 Microscopy, Raman images and Raman spectra of the cancerous breast tissue (infiltrating ductal cancer, G3) of the patient P80. A Microscopy image (500 × 500 μm) composed of several single video images of the cancerous breast tissue, B Raman image (150 × 150 μm) of the cancerous cryosectioned tissue from the region marked in A obtained by basis analysis, C Raman spectra of the cancerous human breast tissue. The colours of the spectra correspond to the colours in the image. Mixed areas are displayed as mixed colours. Integration time: 0.03 s.[36]

One can see from Figures 1 and 2 that the lipid profile in the spectral region 2600-3200 cm^{-1} for noncancerous tissue is dominated by the peaks at around 2854, 2874, 2888 cm^{-1} and the peak at 3009 cm^{-1} (=C-H) is also easy observed. This observation confirms that the lipid profile for the noncancerous tissue is dominated by unsaturated fatty acids and their derivatives (esters for example), while the Raman spectra of the cancerous human breast tissue are dominated by proteins for which the peak at around 2940 cm^{-1} is most characteristic.[36,52-55] To monitor the accumulation and spatial distribution of the individual components in the noncancerous and the cancerous breast tissues: carotenoids, lipids, fatty acids, and proteins Raman filters presented in Figures 3 and 4 were used. The spectral region 1500-1550 cm^{-1} is typical for carotenoids, 2850-2950 cm^{-1} correspond to fatty acids and lipids and 2950-3010 cm^{-1} correspond to proteins and lipids vibrations respectively. The autofluorescence of the tissue was estimated using a filter 1800-2000 cm^{-1}.

Fig. 3 Images for the filters for spectral regions: A 1500–1550 cm^{-1}, B 2850–2950 cm^{-1}, C 2950–3010 cm^{-1} and D 1800–2000 cm^{-1} typical for carotenoids, lipids, proteins vibrations and autofluorescence of the noncancerous human breast tissue, P80.

Fig. 4 Images for the filters for spectral regions: A 1500–1550 cm^{-1}, B 2850–2950 cm^{-1}, C 2950–3010 cm^{-1} and D 1800–2000 cm^{-1} typical for carotenoids, lipids, proteins vibrations and autofluorescence of the cancerous human breast tissue, P80.

The results presented in Figures 3 and 4 clearly indicate that Raman mapping is a suitable technique to monitor qualitatively and quantitatively (the quantitative analysis is beyond the scope of this paper) the composition of human breast tissues and many compounds can be monitored simultaneously. The comparison of the results for different filters shows that in the noncancerous tissue a high level of carotenoids, which are almost absent in a cancerous human breast tissue sample, can be observed. In regions rich in carotenoids high concentration of lipids, fatty acids and their derivatives is also noticed. Simultaneously in samples areas rich in lipids, fatty acids and their derivatives a lower concentration of proteins is observed.

Additionally, the higher fluorescence is typical for the cancerous human breast tissue.

Because we have confirmed that the fatty acids play so important role in cancerogenesis it is reasonable to compare the lipid profile of the cancerous and the noncancerous human breast tissues with the Raman spectra of selected fatty acids: LA and OA. Detailed comparison for Raman spectra of the breast tissues, and selected oleic acid and linoleic acids is presented in Fig. 5.

Fig. 5 Comparison of average Raman spectra of the noncancerous and the cancerous breast tissues of patient P80, oleic and linoleic acids.

One can see from Figure 5 that the average Raman spectrum of the noncancerous human breast tissue contains all bands characteristic for selected unsaturated acids. This observation confirms the indisputable role of these acids in the composition of such type of tissue, originating from adipose tissue content. In contrast such similarities are not observed for the cancerous tissue. Raman spectrum of the cancerous tissue is dominated by a peak at around 2940 cm^{-1} which can be described as a combination of the vibrations of saturated lipids and proteins[35,51] (see Table S1 in the ESI†).

Having reached this point, when we proved that unsaturated fatty acids play a very important role in differentiation of the normal and the pathological changed human breast tissues we can ask the question if we can obtained any information about conformational properties of selected linoleic and oleic acids using Raman spectroscopy.

To gain more information on conformational properties and phase transitions we have investigated Raman spectra of OA and LA as a function of temperature in the range of 293-77 K.

We will demonstrate that the detailed structural evolution of acids chains for LA and OA can be elucidated by analyzing the vibrational spectra of C-H, =C-H and C=C modes. Figure 6 presents the Raman spectra of LA and OA as a function of temperature.

Fig. 6 Raman spectra of LA and OA as a function of the temperature in a spectral range: A: 700-1800 cm^{-1}, B: 2600-3200 cm^{-1}.

Figures 7, 8, 9, 10 present the temperature dependence of the maximum peak positions for LA and OA: $\nu s(CH_2)$, $\nu as(CH_2)$, $\nu s(CH_3)$ stretching modes, and ν(=C-H) vibration.

Fig. 7 The temperature dependence of the maximum peak positions for LA and OA for: $\nu s(CH_2)$ vibration.

Fig. 8 The temperature dependence of the maximum peak positions for LA and OA for: $\nu as(CH_2)$ vibration.

Fig. 9 The temperature dependence of the maximum peak positions for LA and OA for: $\nu s(CH_3)$ vibration.

Fig. 10 The temperature dependence of the maximum peak positions for LA and OA for: νs(=CH) vibration.

The C-H vibrations of the hydrocarbon chains are sensitive to the conformational changes, mobility and disorder-order transitions and usually exhibit distinct temperature induced changes.[35] One can see form Figures 6 and 7, 8, 9, 10 that this indeed happens for LA and OA. From the shifts of the maximum peak positions we can easy identify disorder-order transitions which occur at 222 K and 240 K for LA and at 270 K and 285 K for OA respectively.

For the comparison Figure 11 presents the changes in maximum peak position for C=C band crucial for unsaturated acids chains dynamics.

Fig. 11 Temperature dependence of the maximum peak positions of A:LA, and B: OA for ν_s (C=C) band.

According to the fact that the crystallographic analysis of OA and LA shows that the LT phase of LA has structural features similar to the γ phase of the oleic acid,[56-58] comparison of phase transitions between the α/γ and MT/LT transitions can additionally elucidate how the methylene group interferes diene structure of LA and affects properties of the solid states transitions.

The cell parameters characterizing γ phase of OA and LT phase of LA are summarized Table 1. One can see from Table 1 that cell parameters of OA and LA at low temperatures show many similarities and the comparison of these two phases is highly justified.

Table 1. Cell parameters of OA and LA at low temperatures[50]

acid	Space group	a/Å	b/Å	c/Å	β/deg	V/$Å^3$
OA	$P2_1/a$	9.51	4.74	40.60	~90	~1830
LA	$P2_1/a$	9.37	4.63	42.98	109.38	1761

Figure 12 presents the molecular structures of OA and LA and schematic presentation of geometrical relations between the monoclinic and pseudo-orthorhombic unit cell.

Fig. 12 Molecular structures of OA and LA and schematic presentation of geometrical relations between the monoclinic and pseudo-orthorhombic unit cell.

The structure of the γ phase of OA was determined by Abrahammson and Rydersteht-Nahringbauer.[57] The unit cell of OA consisting of four molecules belongs to the pseudo-orthorhombic system of space group $P2_1/a$ and the internal rotation angles of the two C-C bonds linked to cis C=C are +133°, and -133°, which confirm that two all-trans chains on both sides of cis C=C bond form $O\|'$ subcell in the γ phase.[57]

The structure of the LT phase of the LA was determined by Ernst et al.[58] The unit cell of LA consists of four molecules and like for OA and belongs to space group $P2_1/a$. The internal

rotation angles of the four C-C bonds linked to cis C=C are -119°, and +123°, +124°, and -121° respectively. With these conformations the hydrocarbon chains are parallel to each other and the two hydrocarbon chains are packed in the $O\parallel'$ subcell.[58] Summarizing LA and OA belong to the same space group. Both acids have also a carboxyl side chains consists of seven CH_2 groups. That's why the changes noticed in a maximum peak positions for hydrocarbon chains are observed almost at the same frequencies (Figures 6-11).

From Figures 7-11 one can notice also that for C-H bonds for LA a step decreasing of the maximum peaks position for MT/LT transition with temperature decreasing is observed

Similar step changes were observed for α/γ transitions for OA.

Additionally one can see from Figures 7-11 that the spectral shifts observed for CH vibrations of LA are smaller than those for OA. It indicates that structural changes characteristic for MT/LT transition typical for LA are smaller compared to the α/γ transition typical for OA. This can be due to the fact that the methyl side chain of LA consists of only four CH_2 groups (Figure 12).

In other words the larger part of OA molecule: from the cis-olefine to the methyl part is involved in phase transition. The smaller changes for MT/LT transition for LA are observed also for C=C vibrations on Figure 11. However, for C=C vibration the opposite trend with temperature decreasing was observed.

The difference in the magnitude of the spectral changes discussed above are consistent with thermodynamic data, the transition enthalpy of the MT/LT transition (2.6 kJ/mol) is about one third of those of α/γ transition (8.76 kJ/mol). This relation once again suggests the smaller magnitude of structural changes on the MT/LT transition.

Form Figures 6-11 one can notice also that the phase transitions temperatures typical for LA are also significantly lower (222 K, 240 K) compared to the phase transitions temperatures characteristic for OA (285 K, 270 K). When we combine results indicating smaller structural changes typical for LA transitions with molecular structure of LA and OA and influence of methylene group interrupting diene structure for LA one can summarize that the C-C bonds adjacent to the cis-C=C bond are able to adopt various rotation angles causing a highly flexible nature of these chains and we can regard CH_2 group as highly mobile.

Conclusions

Some important aspects of the Raman microspectroscopy analysis of the noncancerous and the cancerous human breast tissues and phase transitions of LA and OA in the pure state by low-temperatures Raman studies have been reported. Presented studies allow the following conclusions:

1. the Raman images are sensitive indicators of distribution of fatty acids, lipids, proteins and carotenoids in the cancerous and the noncancerous human breast tissues,
2. the noncancerous human breast tissue contains more adipose cells dominated by the unsaturated acids and their derivatives,
3. the temperature dependence of Raman spectra are sensitive indicators of phase transitions of the major components of the tissue,
4. HT/MT, and MT/LT transitions for LA can be identified by Raman spectroscopy,
5. the conformational changes typical for MT/LT transitions of LA are on smaller scale compared to parameters typical for α/γ transition of OA.

Acknowledgements

We thank dr. Jacek Musial MD and prof. dr Radzislaw Kordek MD form Medical University of Lodz for their assistance.
The project was funded through a Dz. St 2014 and The National Science Centre Poland Grant UMO-2012/07/B/ST4/01588.

Notes and references

† Electronic Supplementary Information (ESI) available…

[a] *Lodz University of Technology, Institute of Applied Radiation Chemistry, Laboratory of Laser Molecular Spectroscopy, Wroblewskiego 15, 93-590 Lodz, Poland.*

[*] *To whom correspondence should be addressed: Beata Brozek-Pluska, Lodz University of Technology, Institute of Applied Radiation Chemistry, Laboratory of Laser Molecular Spectroscopy, Wroblewskiego 15, 93-590 Lodz, Poland, telephone number: +48 42 6313188, fax: +48 42 6840043, e-mail: brozek@mitr.p.lodz.pl.*

1. A. H. Lee and N. Hiramatsu, *Nutrition and Dietary Supplements*, 2011, **3**, 93-100.
2. R. K. Murray, D. K. Granner and V. W. Rodwell, *Harper's Biochemistry*, 28ed, The McGraw-Hill Companies, Inc. 2012.
3. B. Brozek-Pluska, J. Musial, R. Kordek, E. Bailo, T. Dieing and H. Abramczyk, *Analyst,* 2012, **137**, 3773-3780.
4. L. Zhou and A. Nilsson, *J. Lipid Res.*, 2001, **42**, 1521–1542
5. C. S. Koble, P. Devchand, W. Wahli, T. M. Willson, J. M. Lenhard and J. M. Lehman, *Proc. Natl. Acad.Sci. USA.*, 1997, **94**, 4318-4323.
6. A. J. Habenicht, P. Salbach and U. Janssen-Timmen, *Eicosanoids,* 1992, **5**, S29-S31.
7. B. Li, C. Birdwell and J. Whelan, *J. Lipid Res.*, 1994, **35**, 1869-1877.
8. H. Harizi, J. B. Corcuff and N. Gualde, *Trends Mol. Med.*, 2008, **14**, 461-469.
9. H. Tapiero, G. Nguyen Ba, P. Couvreur and K. D. Tew, *Biomed. Pharmacother.*, 2002, **56**, 215-222.
10. J. A. Menedez and R. Lupu, *Nature Rev. Cancer*, 2007, **7**, 763-777.
11. T. Mashima, H. Seimiya and T. Tsuruo, *Br. J. Cancer*, 2009, **100**, 1369-1372.
12. C. M. Metallo,. P. A. Gameiro, E. L. Bell, K. R. Mattaini, J. Yang, K. Hiller, Ch. M. Jewell, Z. R. Johnson, D. J. Irvine, Guarente, J K. Kelleher, M. G. Vander Heiden, O. Iliopoulos and G. Stephanopoulos., *Nature*. 2012, **481**, 380-384.
13. A. R. Mullen, W. W. Wheaton, Eunsook S. Jin, P-H Chen, L. B. Sullivan, T. Cheng, Y. Yang, W. M. Linehan, N. S. Chandel and R. J. De Berardinis, *Nature*, 2012, **481**, 385-388.

14. G. Hatzivassiliour, F. Zhao, D. E. Bauer, Ch. Andreadis, A. N. Shaw, D.t Dhanak, S. R. Hingorani, D. A. Tuveson and C. B. Thompson. *Cancer Cell*. 2005, **8**, 311-321.
15. R. Flavin, S. Peluso, P. L Nguyen and M. Loda, *Future Oncol*. 2010, **6**, 551-562.
16. A. Nkondjock and P. Ghadirian, *Canada. Am. J. Clin. Nutr.*, 2004, **79**, 857–864.
17. J. A. Menendez, L. Vellon, R. Colomer and R. Lupu, *Ann. Oncol.*, 2010, **16**, 359–371.
18. E. A. de Deckere, *Eur. J. Cancer Prev.*, 1999, **8**, 213–221.
19. Z. Gu, J. Suburu, H. Chen and Y. Q. Chen, *BioMed Research International*, 2013, 2013, ID 824563, doi:10.1155/2013/824563.
20. F. P. Kuhajda, *Cancer Research*, 2006, **66**, 5977–5980.
21. I. M. Berquin, Y. Min, R. Wu, D. Perry, J. M. Cline, M. J. Thomas, T. Thornburg, G.Kulik, A.Smith, I. J. Edwards, R. D'Agostino, Jr., H. Zhang, H. Wu, J. X. Kang and Y. Q. Chen, *Journal of Clinical Investigation*, 2007, **117**, 1866–1875.
22. C. H. MacLean, S. J. Newberry, W. A. Mojica M. P. H; Puja Khanna, A. M. Issa, M. J. Suttorp, Y.-W. Lim, S. B. Traina, L. Hilton, R. Garland and S. C. Morton, *JAMA,* 2006, **295**, 403–415.
23. P. D. Terry, T. E. Rohan and A. Wolk, *Am. J. Clin. Nutr.*, 2003, **77**, 532–543.
24. J. B. Ewaschuk, M. Newell and C. J. Field, *Lipids*, 2012, **47**, 1019–1030.
25. H. Sun, I. M. Berquin, R. T. Owens, J. T. O'Flaherty and I. J. Edwards, *Cancer Research*, 2008, **68**, 2912–2919.
26. P. D. Schley, H. B. Jijon, L. E. Robinson and C. J. Field, *Breast Cancer Research and Treatment*, 2005, **92**, 187–195.
27. S. I. Grammatikos, P. V. Subbaiah, T. A. Victor and W. M. Miller, *Br J Cancer.*, 1994, **70(2)**, 219–227.
28. J. Bézard, J. P. Blond, A. Bernard and P. Clouet, *Reprod Nutr Dev*., 1994**, 34(6)**, 539-68.
29. N. Salem, In New Protective Roles for Selected Nutrients; Spiller, G. A., Scala, J., Ed.; Alan R. Liss, Inc.: New York, 1989, 109-228.
30. J. Hamilton, R. Greiner, N. Salem and H. Y. Kim, *Lipids*, 2000, **35**, 863-869.
31. K. Olbrich, W. Rawicz, D. Needham and E. Evans, E. *Biophys. J.*, 2000, 79, 321-327.
32. W. Rawicz, K. Olbrich, T. McIntosh, D. Needham and E. Evans, *Biophys. J.*, 2000, **79**, 328-339.
33. S. E. Carlson, *Am. J. Clin. Nutr*., 2000, 71, 268-274.
34. H. Abramczyk, B. Brozek-Pluska, J. Surmacki, J. Jablonska-Gajewicz and R. Kordek, *Prog. Biophys. Mol. Biol.*, 2012, **108**, 74–81.
35. B. Brozek-Pluska, J. Jablonska-Gajewicz, R. Kordek and H. Abramczyk, *J. Med. Chem.*, 2011, **54**, 3386–3392.
36. B. Brozek-Pluska, J. Musial, R. Kordek**,** E. Bailo, Th. Dieing and H. Abramczyk, *Analyst*, 2012, **137**, 3773-3780.
37. M. Iwahashi, Y. Yamaguchi, T. Kato, T. Horiuchi, I. Sakurai and M. Suzuki, *J. Phys. Chem.*, 1991, **95**, 445– 451
38. M. Iwahashi, N. Hachiya, Y. Hayashi, H. Matsuzawa, M. Suzuki, Y. Fujimoto and Y. Ozaki, *J. Phys. Chem.*, 1993, **97**, 3129-3133.
39. M. Iwahashi, Y. Kasahara, H. Matsuzawa, K. Yagi, K. Nomura, H. Terauchi, Y. Ozaki and M. Suzuki, *J. Phys. Chem*,. 2000, **104**, 6186-6194.
40. F. Kaneko, J. Yano and K. Sato, *Curr. Opin. Struct. Biol.*, 1998, **8**, 417-425.
41. F. Kaneko, K. Yamazaki, K. Kitagawa, T. Kikyo, M. Kobayashi and Y. Kitagawa, *J. Phys. Chem.*, 1997, **101**, 1803-1809.
42. S. Abrahamsson, B. Dahlen, H. Lofgren and J. Pascher, *Prog. Chem. Fats Other Lipids,* 1978, **16**, 125-143.
43. F. Kaneko, K. Tashiro and M. Kobayashi, *J. Cryst. Growth*, 1999, **198-199**, 1352-1359.
44. M. Kobayashi, F. Kaneko, K. Sato and M. Suzuki, *J. Phys. Chem.*, 1986, **90**, 6371-6378.
45. S. P. Verma and D. F. H. Wallach, *Biochem. Biophys. Acta*, 1977, **486**, 217-227.
46. Y. Kim, H. L. Strauss and R. G. Snyder, *J. Phys. Chem.*, 1988, **92**, 5080-5082.
47. S. Ueno, A. Miyazaki, J. Yano, Y. Furukawa, M. Suzuki and K. Sato, *Chem. Phys. Lipids*, 2000, **107**, 169-178.
48. M. Suzuki, K. Ogaki and K. Sato, *J. Am. Oil Chem. Soc*., 1985, **62**, 1600-1604.
49. K. Sato and M. Suzuki, *J. Am. Oil Chem. Soc*., 1986, **63**, 1356-1359.
50. F. Pi, F. Kaneko, M. Iwahashi, M. Suzuki and Y. Ozaki, *J. Phys. Chem. B*, 2011, **115***,* 6289-6295.
51. H. Abramczyk, B. Brozek-Pluska, J. Surmacki, J. Musial and R. Kordek, *Analyst*, 2014, **139**, 5547-5559.
52. G. Hudelist, Ch. F. Singer, K.I. D. Pischinger, K. Kaserer, M. Manavi, E. Kubista and K. F. Czerwenka, *Proteomics* 2006, **6,** 1989-2002.
53. H. Hondermarck, A. S. Vercoutter-Edouart, F. Revillion, J. Lemoine J, I. el-Yazidi-Belkoura, V. Nurcombe and J. P. Peyrat, *Proteomics*. 2001, **1**, 1216-1232.
54. C. P. Paweletz, B. Trock, M. Pennanen, T. Tsangaris, C. Magnant, L. A. Liotta and E. F. Petricoin, *Dis. Markers*. 2001, **17**, 301-307.
55. R. A. Harris, A. Yang, R. C. Stein, K. Lucy, L. Brusten, A. Herath R. Parekh, M. D. Waterfield, M. J. O'Hare, M. A. Neville, M. J. Page and M. J. Zvelebil, *Proteomics*., 2002, **2**, 212-223.
56. The physical chemistry of lipids; Small, D. M., Eds.; Plenum: New York, 1986.
57. S. Abrahamson and I. R. Nahringbauer, *Acta Crystallogr*., 1962, **15**, 1261-1268.
58. J. Ernst, W. S. Sheldrick, and J-H. Fuhrhop, Z. Naturforsch., 1979, **34b**, 706-711.

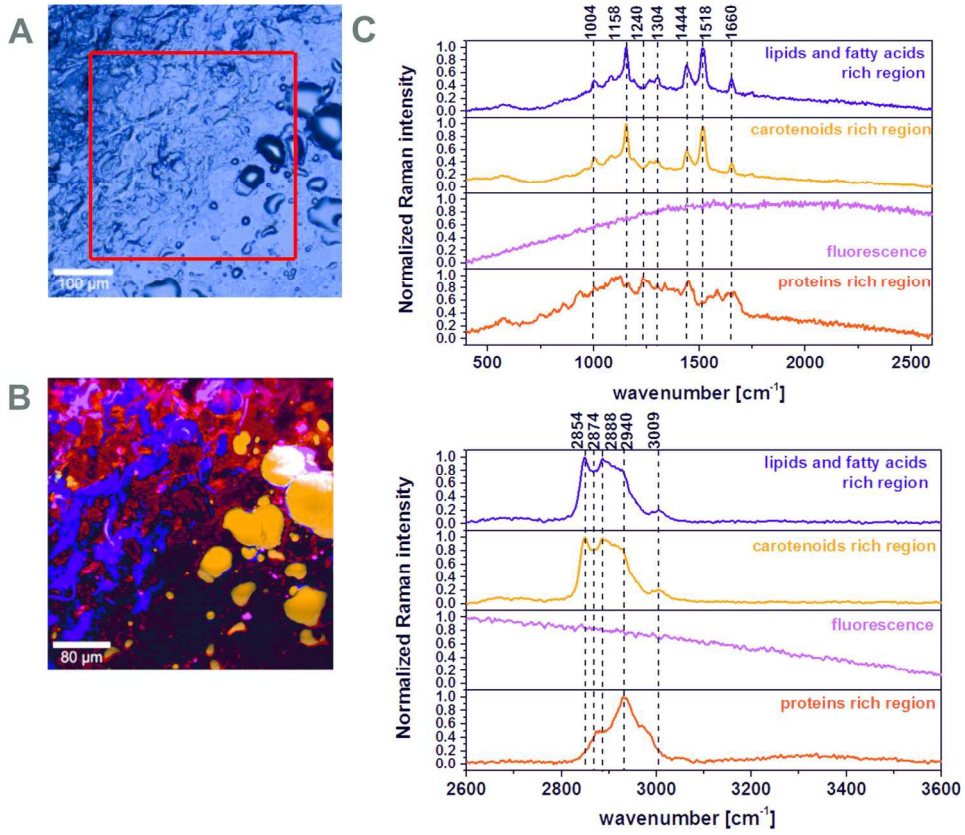

Fig. 1 Microscopy, Raman images and Raman spectra of the noncancerous breast tissue of patient P80. A Microscopy image (500 × 500 µm) composed of several single video images of the noncancerous breast tissue, B Raman image (350 × 350 µm) of the cryosectioned noncancerous tissue from the region marked in A obtained by the basis analysis, C Raman spectra of the noncancerous breast tissue. The colours of the Raman spectra correspond to the colours in the Raman image. Mixed areas are displayed as mixed colours. Integration time: 0.03 s.36
161x141mm (300 x 300 DPI)

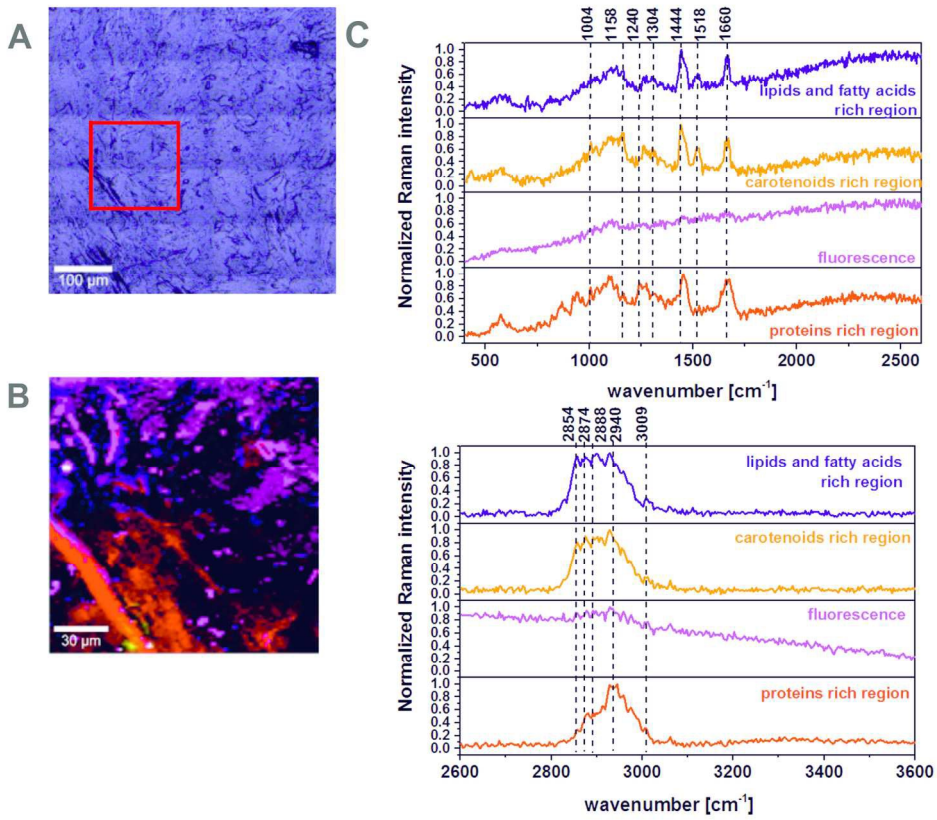

Fig. 2 Microscopy, Raman images and Raman spectra of the cancerous breast tissue (infiltrating ductal cancer, G3) of the patient P80. A Microscopy image (500 × 500 µm) composed of several single video images of the cancerous breast tissue, B Raman image (150 × 150 µm) of the cancerous cryosectioned tissue from the region marked in A obtained by basis analysis, C Raman spectra of the cancerous human breast tissue. The colours of the spectra correspond to the colours in the image. Mixed areas are displayed as mixed colours. Integration time: 0.03 s.36
161x140mm (300 x 300 DPI)

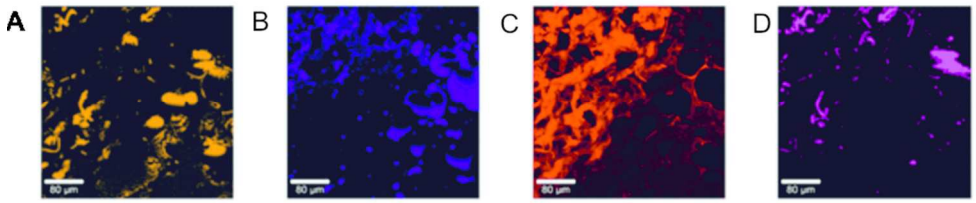

Fig. 3 Images for the filters for spectral regions: A 1500–1550 cm−1, B 2850–2950 cm−1, C 2950–3010 cm−1 and D 1800–2000 cm−1 typical for carotenoids, lipids, proteins vibrations and autofluorescence of the noncancerous human breast tissue, P80.
82x17mm (300 x 300 DPI)

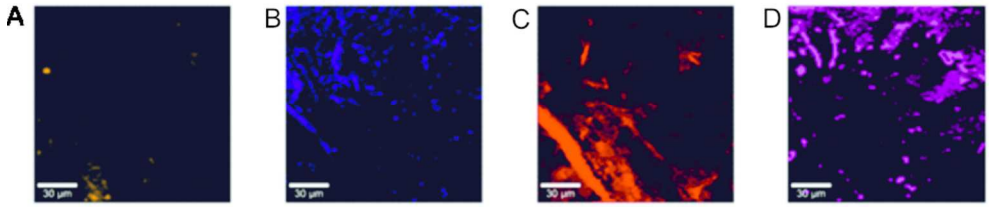

Fig. 4 Images for the filters for spectral regions: A 1500–1550 cm−1, B 2850–2950 cm−1, C 2950–3010 cm−1 and D 1800–2000 cm−1 typical for carotenoids, lipids, proteins vibrations and autofluorescence of the cancerous human breast tissue, P80.
82x17mm (300 x 300 DPI)

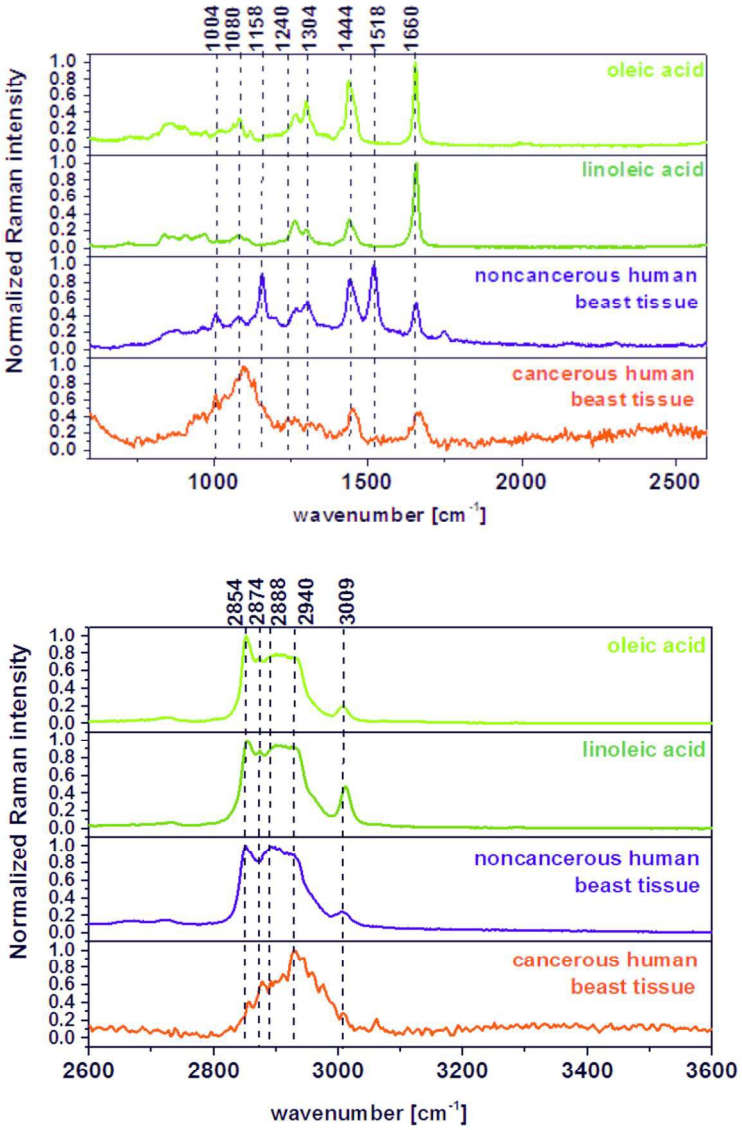

Fig. 5 Comparison of average Raman spectra of the noncancerous and the cancerous breast tissues of patient P80, oleic and linoleic acids.
161x217mm (300 x 300 DPI)

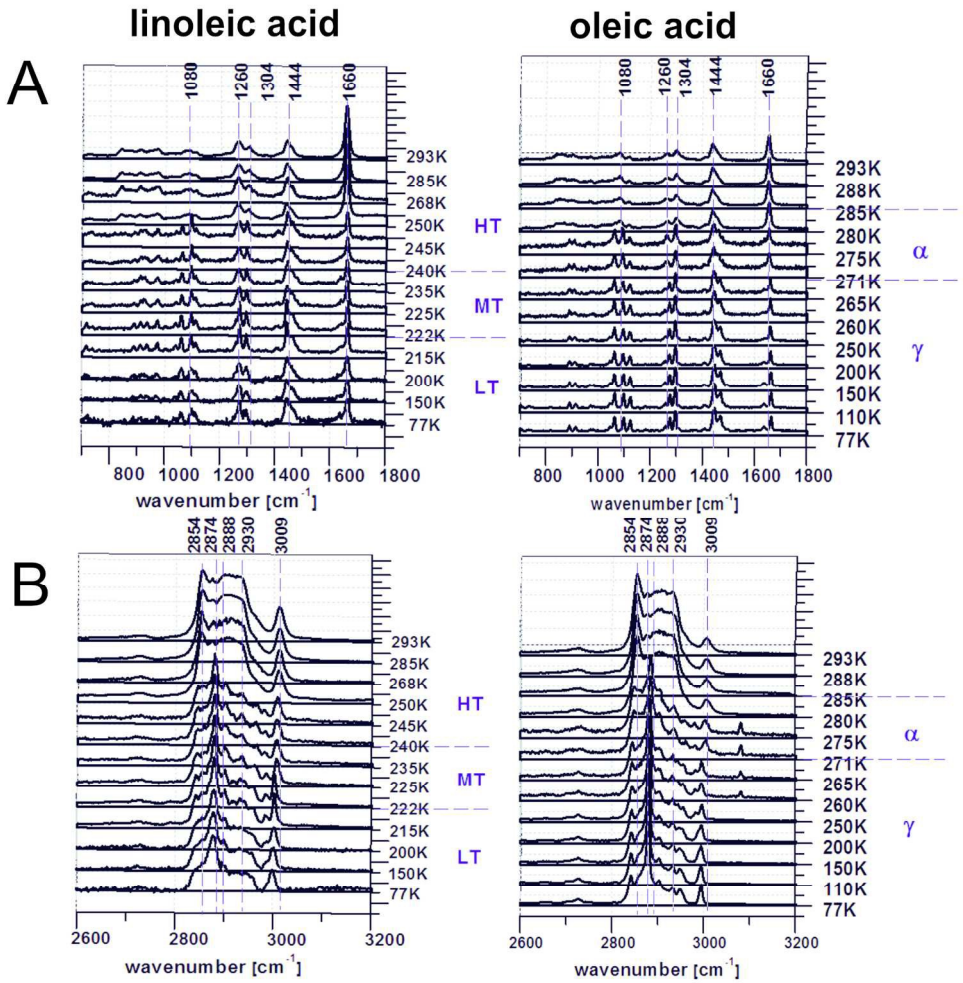

Fig. 6 Raman spectra of LA and OA as a function of the temperature in a spectral range: A: 700-1800 cm-1, B: 2600-3200 cm-1.
161x162mm (300 x 300 DPI)

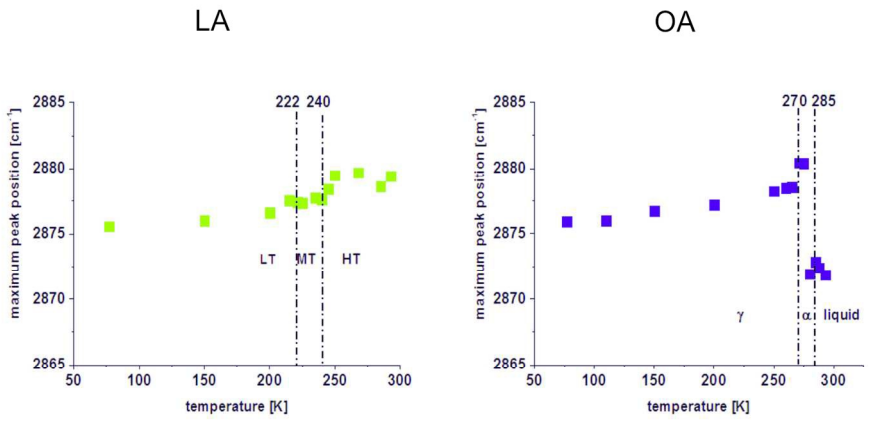

Fig. 7 The temperature dependence of the maximum peak positions for LA and OA for: vs(CH2) vibration.
161x77mm (300 x 300 DPI)

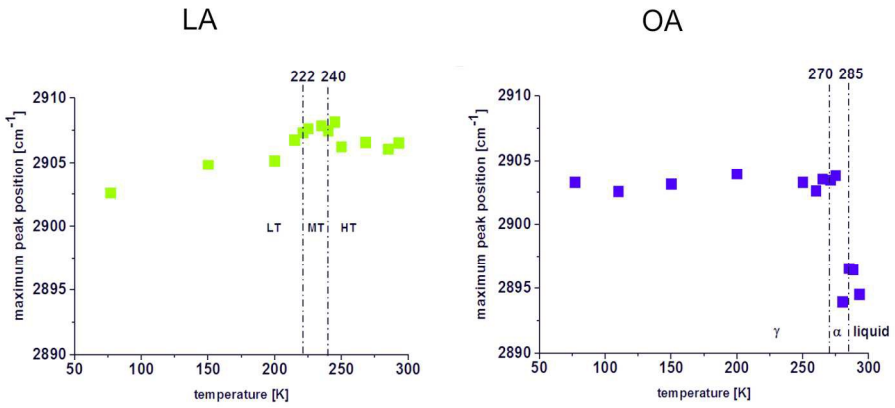

Fig. 8 The temperature dependence of the maximum peak positions for LA and OA for: vas(CH2) vibration.
161x77mm (300 x 300 DPI)

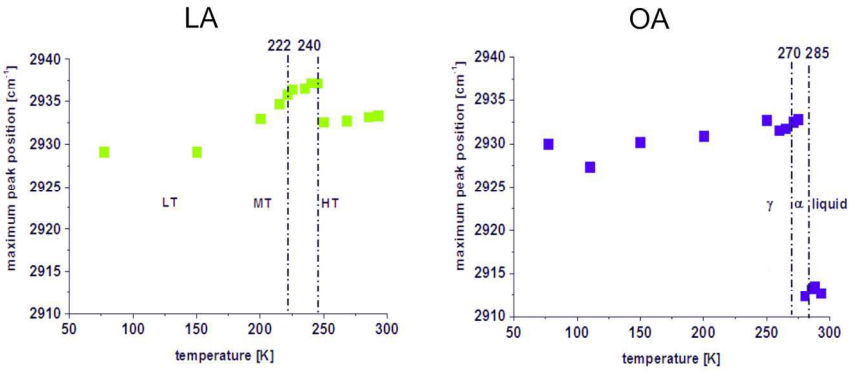

Fig. 9 The temperature dependence of the maximum peak positions for LA and OA for: vs(CH3) vibration.
161x65mm (300 x 300 DPI)

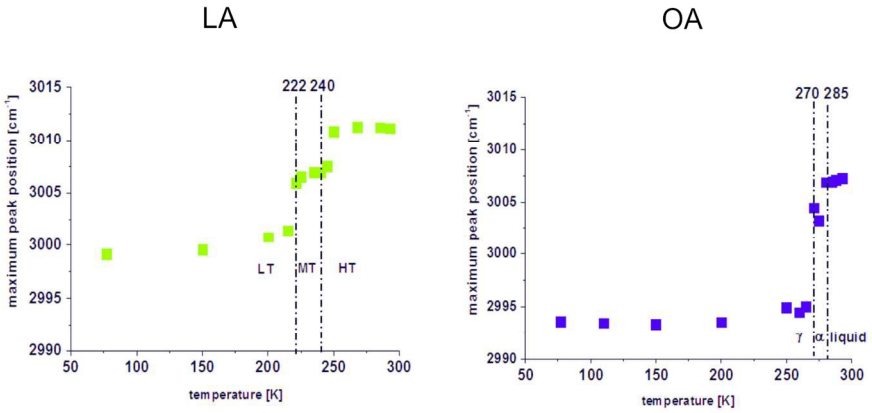

Fig. 10 The temperature dependence of the maximum peak positions for LA and OA for: vs(=CH) vibration.
161x77mm (300 x 300 DPI)

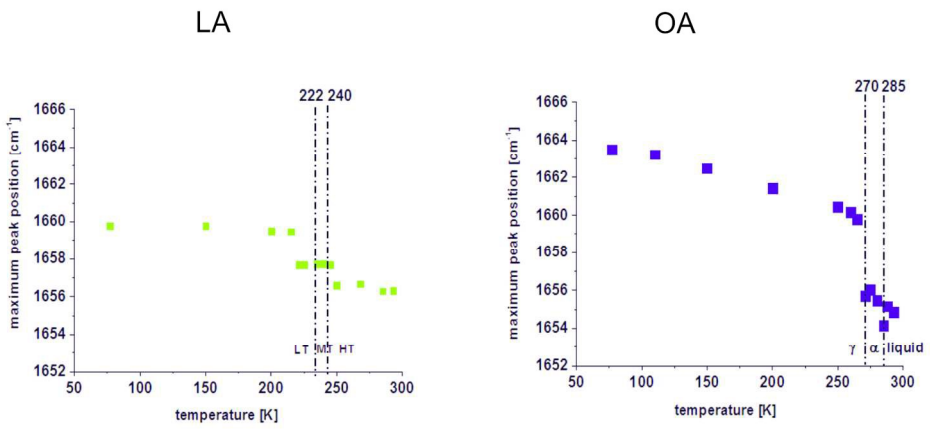

Fig. 11 Temperature dependence of the maximum peak positions of A:LA, and B: OA for vs (C=C) band.
161x77mm (300 x 300 DPI)

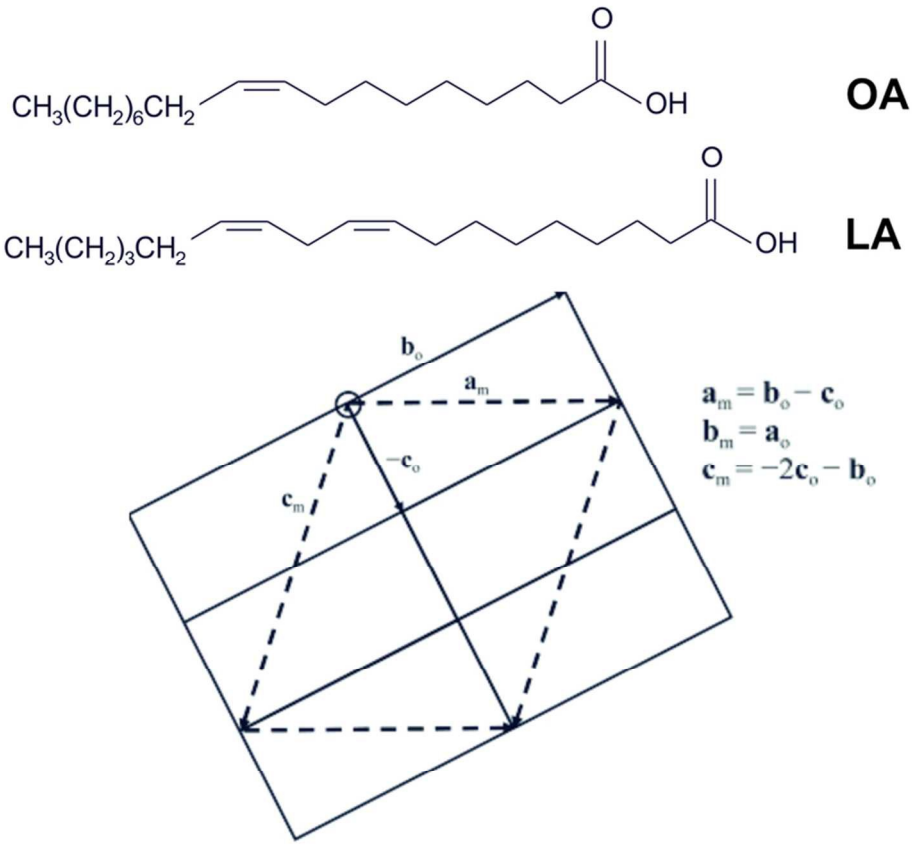

Fig. 12 Molecular structures of OA and LA and schematic presentation of geometrical relations between the monoclinic and pseudo-orthorhombic unit cell.
75x68mm (300 x 300 DPI)